

Bursting emission from PSR B0611+22

A. D. Seymour^{1*}, D. R. Lorimer^{1,2,3} and J. P. Ridley⁴

¹*Department of Physics, West Virginia University, Morgantown, WV 26505, USA*

²*National Radio Astronomy Observatory, Green Bank, WV 24944, USA*

³*Astrophysics, University of Oxford, Denys Wilkinson Building, Keble Road, Oxford OX1 3RH*

⁴*Department of Engineering and Physics, Murray State University, Murray, KY 42071, USA*

Accepted; 10 February 2014

ABSTRACT

Over the past decade it has become apparent that a class of ‘bursting pulsars’ exist with the discovery of PSR J1752+2359 and PSR J1938+2213. In these pulsars, a sharp increase in the emission is observed that then tends to systematically drop-off from pulse-to-pulse. In this paper we describe the discovery of such a relationship in high-sensitivity observations of the young (characteristic age of 90,000 yrs) 0.33 s pulsar B0611+22 at both 327 MHz and 1400 MHz with the Arecibo radio telescope. While Nowakowski previously showed that B0611+22 has mode-switching properties, the data presented here show, for the first time, that this pulsar emits bursts with characteristic time-scales of several hundred seconds. At 327 MHz, the pulsar shows steady behaviour in one emission mode which is enhanced by bursting emission slightly offset in pulse phase from this steady emission. Contrastingly at 1400 MHz, the two modes appear to behave in a competing operation while still offset in phase. Using a fluctuation spectrum analysis, we also investigate each mode independently for sub-pulse drifting. Neither emission mode (i.e. during bursts or persistent emission) shows the presence of the drifting sub-pulse phenomenon. The bursting phenomena seen here appears to be a hybrid between bursting seen in other pulsars and the bistable profile illumination behaviour reported in two other pulsars by Rankin et al. Further examples of this cross-frequency behaviour are required, as this phenomenon may be quite common among the pulsar population.

Key words: methods: data analysis – pulsars: general – pulsars: individual: B0611+22

1 INTRODUCTION

High-precision timing observations which probe neutron star physics, general relativity, and other phenomena rely on tracking rotational phase as measured by template matching of stable integrated pulse profiles (for a discussion, see Lorimer & Kramer 2005). Upon closer examination, however, the radio emission displays a rich variety of examples in which pulsars appear to flip between various states on a wide range of timescales.

Shortly after the discovery of pulsars, in a remarkable series of papers making use of the Arecibo telescope, Backer (1970b,d,a,c) showed that pulsars exhibit nulling, mode-changing and sub-pulse drifting phenomena in their pulse-to-pulse emission. Nulling, the abrupt halting of the emission mechanism for a few or many hundreds of pulses (Backer 1970d) can, be viewed as an extreme version of mode-changing (Backer 1970b,a,c) during which the pulse

profile exhibits two or more stable pulse shapes. Although not universal, an analysis of pulse nulling across the population of isolated pulsars by Wang et al. (2007) tends to suggest that the fraction of time spent in the null state increases with characteristic age. Sub-pulse drifting (Drake & Craft 1968; Backer et al. 1973), where clearly ordered subpulses drift across the main pulse window at a fixed rate characterized by a subpulse spacing and a repetition period appeared to be preserved over an interval of time spent in the null state (Unwin et al. 1978).

With the passage of time, more discoveries have blended and questioned these classifications. Huguenin et al. (1970) discovered the first of a number of pulsars that appear to combine mode changing with sub-pulse drift, where these pulsars generally assume one of several sub-pulse drifting modes.

Also, Rankin et al. (2006) have shown that some pulsars exhibit what they term “bistable profile illumination”, which is single-pulse drifting that mimics the abrupt beginnings of mode-changing but then gradually drifts into phase with

* E-mail: aseymour@mix.wvu.edu

the normal mode. Wang et al. (2007) suggest that nulling and mode changing are different manifestations of the same phenomenon.

Other extraordinary pulsars that may relate nulling to mode-changing occur on a wide range of timescales. A few of these discoveries have been the rotating radio transients (RRATs; McLaughlin et al. (2006)), the intermittent pulsars (Kramer et al. 2006; Camilo et al. 2012; Lorimer et al. 2012) and the observation of bursting emission, which was until now only seen in J1752+2359 (Lewandowski et al. 2004) and J1938+2213 (Chandler 2003; Lorimer et al. 2013). The bursting pulsars bear some resemblance to conventional nulling pulsars, with the exception that the pulse to pulse intensities are modulated by a decaying envelope before abruptly returning to a null or faint state. While the RRATs emit only occasional individual pulses spaced anywhere between seconds and years, intermittent pulsars switch on and remain steady before switching off again over timescales of days to years. Over these longer timescales, where it is possible to measure the spin period derivative precisely, it is observed that the “on” and “off” states for the intermittent pulsars are associated with two different spin-down rates (Kramer et al. 2006).

A similar behaviour was recently seen in 17 non-intermittent pulsars (Lyne et al. 2010) which switch between different spin-down states in a quasi-periodic or even chaotic fashion (Seymour & Lorimer 2013), and are sometimes accompanied by correlated pulse profile changes. Lyne et al. (2010) suggest that the mixture of spin-down states could even account for the “timing noise” variations seen in many pulsars and suggest that most, if not all, normal pulsars have multiple spin-down states indicating global changes in magnetospheric current densities. One implication of these results is that mode changing (and perhaps, by association, bursting) could be connected to spin-down rate changes on much shorter timescales. Very recently, synchronous X-ray and radio state switching was reported in the classical mode-changing pulsar B0943+10 (Hermesen et al. 2013). In this case, non-thermal unpulsed X-rays are observed during the bright radio emitting phases, while an additional pulse thermal component is present during the radio-quiet phase. A better understanding of the observational phenomenology involved is now required in order to make further progress.

In this paper, we present a previously unseen bursting emission phenomenon in PSR B0611+22 which was discovered by Davies et al. (1972). This young pulsar with a characteristic age of 90,000 years, has considerably high timing noise (Helfand et al. 1980). This high level of noise could indicate that there is still some underlying phenomena that is not being accounted for in the timing models. At first glance, it appears to be a normal pulsar with a simple pulse shape - essentially Gaussian in appearance that is approximately 80% linearly polarized (Rankin et al. 1989). Yet, it has been shown that the integrated pulse shape varies at different times (Ferguson & Boriakoff 1980). Nowakowski (1992) has also shown that there is a correlation with the brighter pulses and their phase alignment, and later claimed that the timing noise was due to mode switching (Nowakowski & Rivera 2000). Other efforts have been made to find a relationship contributing to this timing noise, such as sub-pulse drifts (Weltevrede et al. 2007), but to no avail.

In this paper, using archival Arecibo observations, we have been able to reveal that this pulsar exhibits bursting episodes and confirm that it has moding behaviours. How this was performed and the implications are outlined in this paper in the following way. In Section 2 we provide technical information about the observations. In Section 3 we detail the data analysis techniques used to expose relationships from pulse-to-pulse. In Section 4 we conduct a fluctuation spectrum analysis on the normal and bursting modes found in Section 3. In Section 5, motivated by the recent X-ray observations of PSR B0943+10, we make predictions for observations of B0611+22 at X-ray wavelengths that may help to understand the phenomenon seen here. Finally, in Section 6, we discuss our results and their scientific significance.

2 OBSERVATIONS

The data presented here were collected between March 2 and 8, 2009 (MJD range 54892–54898) in a dedicated observing run with the Arecibo telescope to search for unusual spectral index behaviour in PSR B0611+22. To characterize the flux density spectrum, observations were carried out at 327 MHz, 1400 MHz, 4.5 GHz, and 8.8 GHz using the Wide Band Arecibo Pulsar Processors (WAPPs; Dowd et al. 2000). Unfortunately, the pulsar was not detected at 8.8 GHz and radio frequency interference (RFI) dominated the 4.5 GHz observations. Further details on the individual observations in which the pulsar was clearly detected are shown in Table 1.

3 DATA ANALYSIS

The data from each of the observations listed in Table 1 were analyzed in a systematic way, as described below.

3.1 Individual pulse profiles

The autocorrelation functions recorded by the WAPPs in each polarization channel were summed and Fourier transformed to convert them to the equivalent set of total-power spectral channels using standard data analysis techniques (see, e.g., Section 5.2.2 of Lorimer & Kramer 2005) implemented in the `filterbank` program as part of the SIGPROC¹ pulsar processing package. The resulting data were then dedispersed at the pulsar’s dispersion measure ($96.91 \text{ cm}^{-3} \text{ pc}$) and folded at the predicted pulse period (0.33 s) using the ephemeris provided in the ATNF pulsar catalog (Manchester et al. 2005)². The SIGPROC `fold` program was used to produce an ASCII pulse profile with 256 rotational phase bins. Then using the standard deviation of the off-pulse bins, we were able to convert to mJy using the radiometer equation (see, e.g., Section 7.3.2 of Lorimer & Kramer 2005), with a gain of 10 K/Jy and an assumed system temperature of 122 K for 327 MHz and 30 K for 1.4 GHz. Zoomed-in versions of these profiles are shown in the left panels of Figs. 1 and 3.

¹ <http://sigproc.sourceforge.net/>

² www.atnf.csiro.au/people/pulsar/psrcat/

Table 1. Summary of Arecibo observations of B0611+22.

MJD	Centre Frequency (MHz)	Integration Time (s)	Bandwidth/Channel (MHz)	Sample time (μ s)	Number of Channels
54892.97	1400	900	0.195	256	2048
54893.01	327	900	0.012	256	4096
54894.95	327	900	0.012	256	4096
54894.97	1400	900	0.781	128	512
54896.94	327	900	0.012	256	4096
54896.97	1400	900	0.781	128	512
54898.95	1400	900	0.781	128	512
54898.97	327	900	0.012	256	4096

3.2 Revealing the emission modes

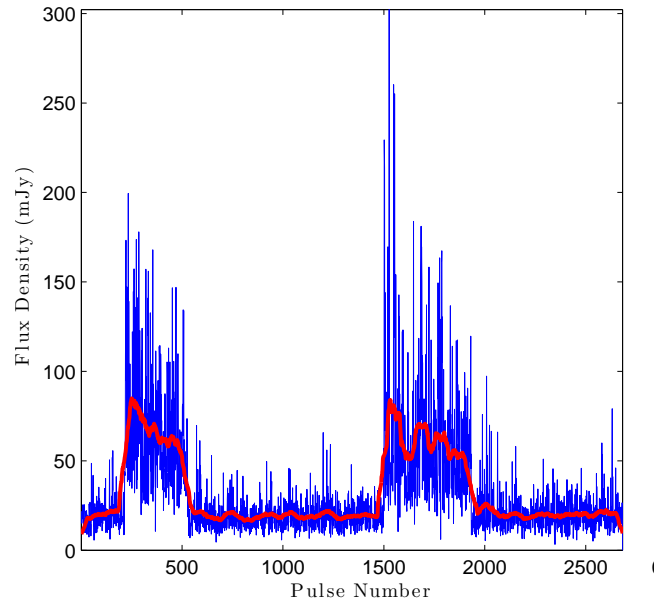
When looking for a relationship across pulse intensities, there is often a great deal of noise present in the system which may obscure any underlying correlation. A simple way to reveal these relationships is to take a boxcar convolution (a running average) over several data points. This method increases the signal-to-noise ratio by the square root of the total number of data points that were averaged, but one must be aware that this will also reduce the resolution of the data along the direction of the averaging. We carried out a boxcar convolution of the data with a normalised area kernel along 64 data points in a single bin, to preserve the bin resolution. We chose this kernel size to reduce the noise fluctuations by at least a factor of five, and to have a multiple of two for computing efficiency. This averaging is often known as smoothing, and we will refer to these post-processed data as smoothed data.

When smoothing is performed on the 327 MHz emission from PSR B0611+22, the mode changes suggested in Nowakowski (1992) are readily apparent, which is shown in the centre panel of Fig. 1. There, two prolonged episodes of enhanced emission can be seen. These enhanced emission episodes can then be isolated when the average of each bin is subtracted from that bin to form the perturbations about the mean. These perturbations are then smoothed to produce the right panel of Fig. 1. It appears that the enhanced episodes are additional effects overlying a normal emission mode.

To examine the structure of these episodes, a bin was chosen in a section where the abnormalities are the dominant feature. The flux density and its convolution for that bin are shown in Fig. 2. There, a decaying behaviour can be seen across the event before it abruptly returns to the normal emission mode. This trend has not been recorded for this pulsar before but is strikingly similar to what was reported in Lewandowski et al. (2004) for PSR J1752+2359. There the authors describe this type of event as bursting. We adopt this nomenclature and will refer to this type of event as a *bursting* emission mode.

To investigate whether these modes can be seen at other frequencies, the same analysis was conducted on data collected at 1.4 GHz. From the perturbations about the mean at this frequency, seen in Fig. 3, it becomes clear that there is an undulating relationship. This suggests that mode switching is present.

To examine whether the structure of these modes are similar to the ones at 327 MHz, we plot bin values from ei-

**Figure 2.** Flux along the bin where the bursting events dominate in Fig. 1. The solid line is the boxcar convolution of the series.

ther side of the undulation which are shown in Fig. 4. On the left side of the undulation, shown in the top of Fig. 4, pulse sequences of larger flux density are mesa (i.e. table-top) shaped with a quite constant mean value throughout before quickly returning to a baseline value. On the other hand, the right-sided enhanced sequences, shown in the bottom of Fig. 4, appear to have the decaying structure of the bursting mode.

This therefore confirms that the two modes found at 327 MHz are also present at 1.4 GHz, but with intriguing differences. Most notably, at 1.4 GHz the bursting mode in the right hand bin is no longer accompanied by a steady weaker mode in the left hand bin. In top of Fig. 4 we can see that the left bin is far from steady and at this higher frequency it exhibits abrupt changes of its own. Moreover, the left hand bursts alternate abruptly with those of the right shown in bottom panel of Fig. 4. Together these form the undulating pattern in Fig. 3.

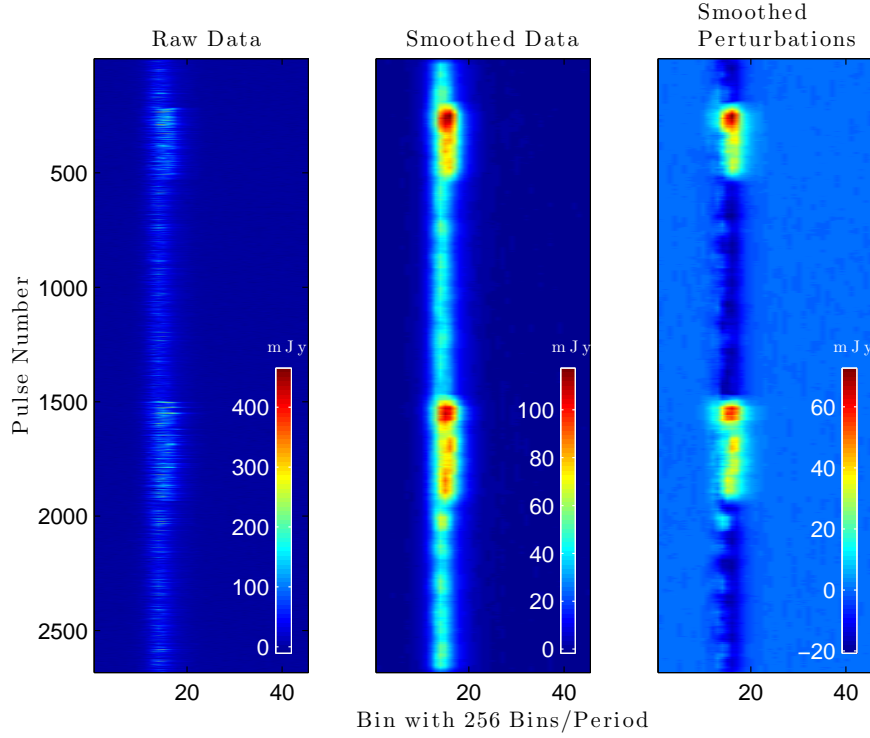


Figure 1. The 327 MHz observation of PSR B0611+22 on MJD 54898. Left: the folded dedispersed time series. Centre: the time series after being box-car convolved along each bin with a kernel of 64 pulses. Right: the convolution of the perturbations about the mean profile with the same kernel.

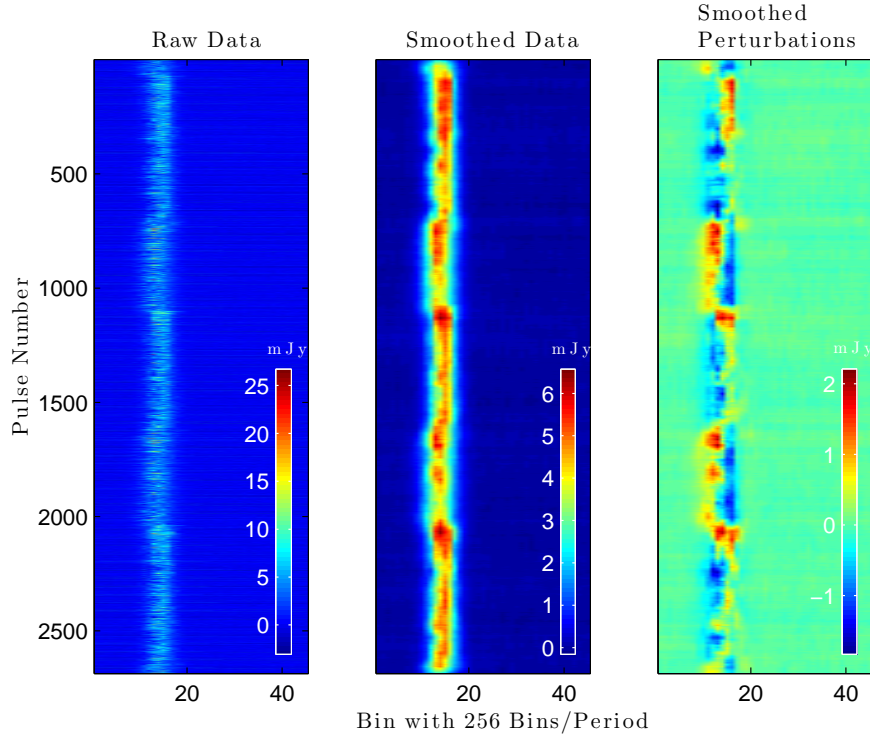


Figure 3. The 1.4 GHz observation of PSR B0611+22 on MJD 54898. Left: The folded dedispersed time series with one pulse profile for each pulse. Centre: the time series after being box-car convolved along each bin with a kernel of 64 pulses. Right: the convolution of the perturbations around the mean profile with the same kernel.

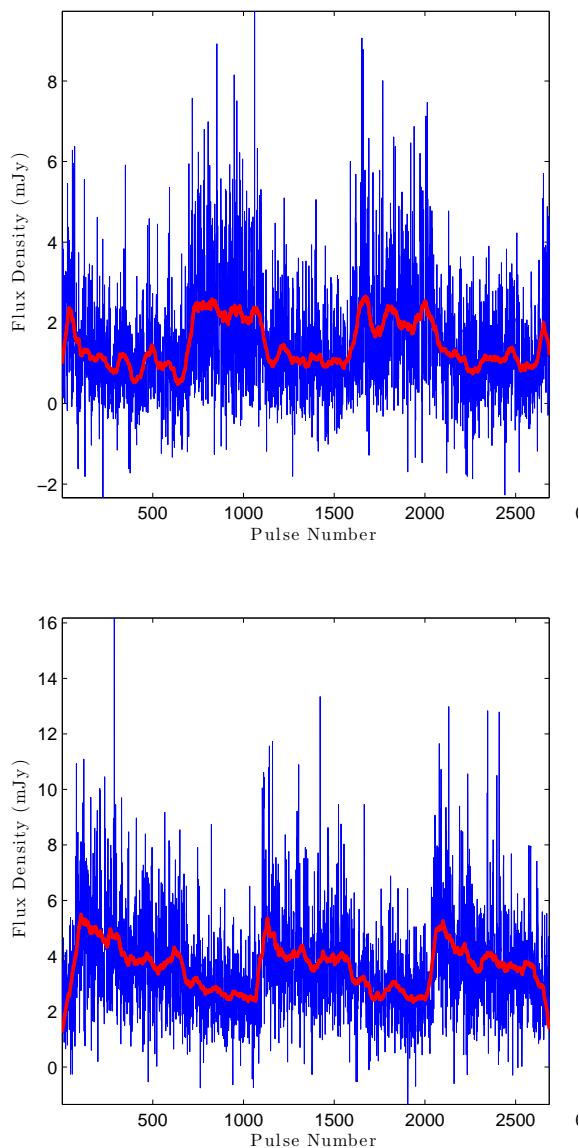


Figure 4. A 15 minute 1.4 GHz observation of PSR B0611+22 on MJD 54898. (*Top*): The flux within a bin where the left-sided fluctuations dominate in Fig. 3. (*Bottom*): The flux within a bin where the right sided fluctuations dominate. The solid line in both is the boxcar convolution of the time series. Note the alternating flux densities between the left and right sided bins

3.3 Gaussian fitting and skewness measurements

To quantify the bursting phenomenon, knowing that the pulse is well described by a Gaussian (Weisberg et al. 1999), we fit Gaussians to each profile on data values greater than 25% of the maximum value of each local mean pulse. This is done to ensure that the fit conforms around the peak of the pulse, and to reduce any asymmetric influences. The resulting fit parameters (peak location μ , amplitude A , and pulse width σ) of each pulse can then be compared to see if changes occur between the two emission modes.

To quantify any asymmetry in the data, we measured the *skewness* of each pulse. This procedure is outlined in

the Appendix. In this calculation, to avoid contamination by noise, only flux density levels greater than 5% of the maximum pulse value are used.

3.3.1 Gaussian and skewness results

Note that, due to the smoothing of the data, any structures on scales smaller than 64 pulse numbers in these results must be treated as a noise feature. For this reason, histograms are generated for each parameter value in order to investigate broader statistical trends.

The results from this analysis of the 327 MHz data are shown in Fig. 5. There, a clear bimodal distribution is seen in the peak locations (μ) histogram. These values are then plotted against pulse number, the lower graph in the μ column of Fig. 5. It then quickly becomes evident that the larger values of μ are associated with the bursting pulses. This directly conveys a phase-shift between the two emission modes.

To isolate the two populations, we set a threshold around the midpoint (at bin 14.9) on the μ values. Pulse numbers with μ values below this threshold are labeled as a normal pulse, and the rest are labeled as a bursting pulse. From this indexing, sub-set histograms are formed for the other recorded parameter values to see how these emission modes contribute to each distribution.

For the pulse width (σ) values measured in the 327 MHz data, there is little that distinguishes the two modes, while the amplitude values (A) are dominated at the higher end by the bursting mode. This is congruent to what was seen in the smoothed data set for this frequency, seen in Fig. 1 and again in the far right of Fig. 5. When these amplitude values are plotted against the pulse number, the lower graph in the A column of Fig. 5, the decaying behaviour mimics what was seen in Fig. 2. This confirms that this decay is an overall effect on the pulse and not a single bin phenomenon. Skewness measurements at 327 MHz show a clear separation between the two modes, and the bursting pulses tend to have a lower skewness than the normal mode.

We also wish to see if these trends are apparent in the pulse profiles. To do this, pulses from the raw data were averaged over the pulse numbers of the corresponding modes and over the whole observation for comparison. These profiles are shown in Fig. 5. There we can see that the mean bursting pulse is indeed larger in amplitude, similar in width, and its peak is slightly shifted compared to the mean normal pulse.

To see if these trends are consistent at other frequencies, the analysis was performed on the 1.4 GHz observation from the same day, shown in Fig. 6. Again we see a clear bimodal distribution in the μ values. When plotted against pulse number, a noticeable phase shift is seen that corresponds with the undulation observed in the smoothed perturbations of Fig. 3. Again, a μ threshold about the midpoint (at bin 14.1) was set to isolate the two modes for comparison.

When these σ values are compared, it is seen that the bursting pulses tend to be narrower than the normal pulses. This trend was not seen in the 327 MHz data, along with little distinction in the amplitude. On the other-hand, the bursting pulses still have the tendency towards lower skewness values.

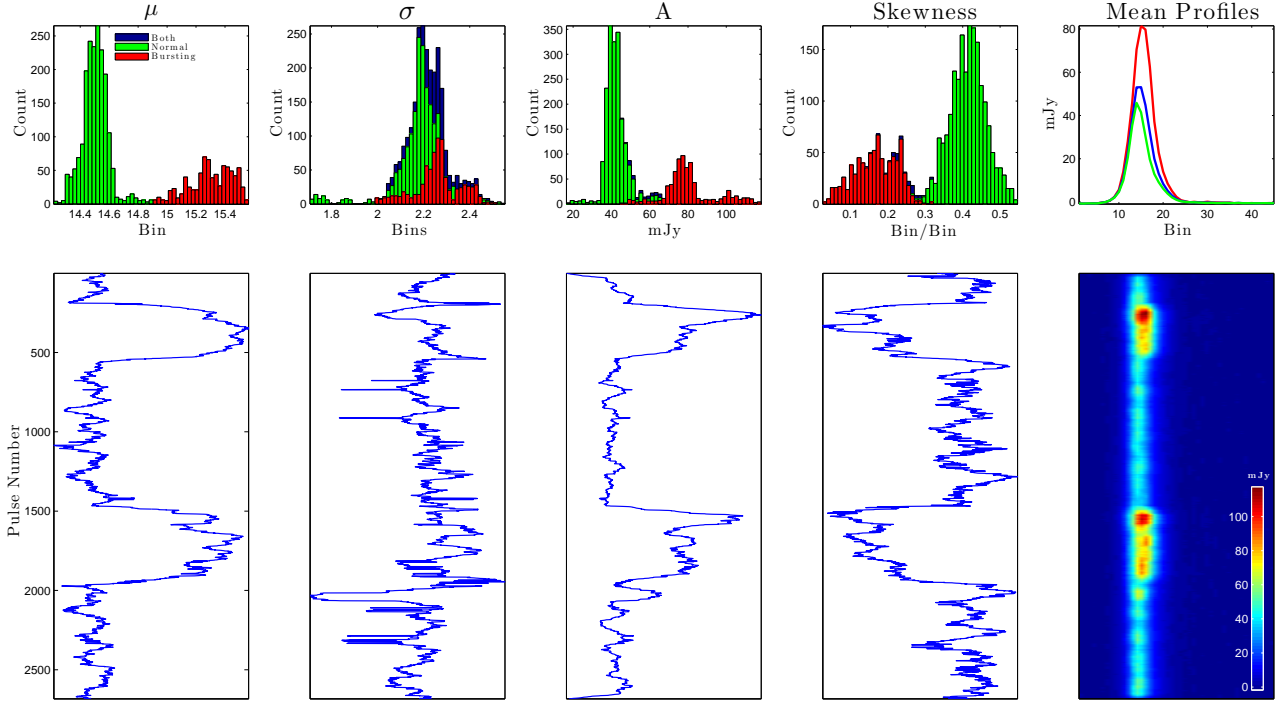


Figure 5. Gaussian parameters and skewness measurements of the smoothed data from the observation carried out on MJD 54898 at 327 MHz.

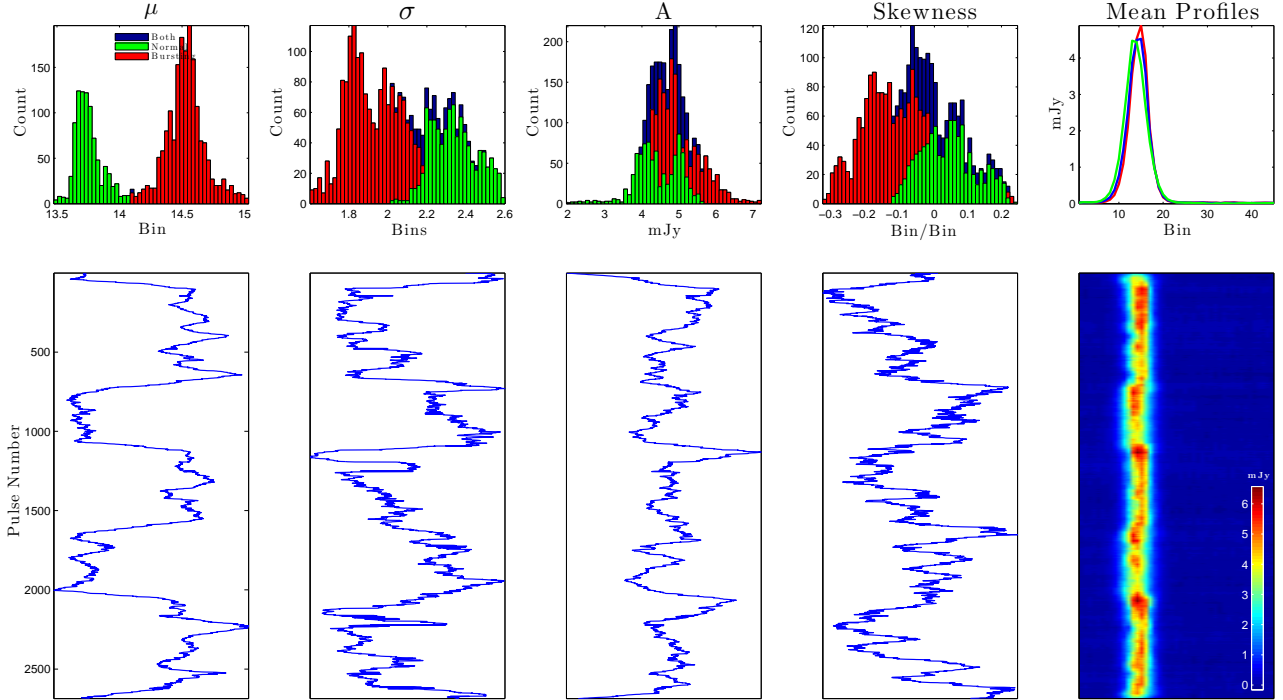


Figure 6. Gaussian parameters and skewness measurements of the smoothed data from the observation carried out on MJD 54898 at 1.4 GHz.

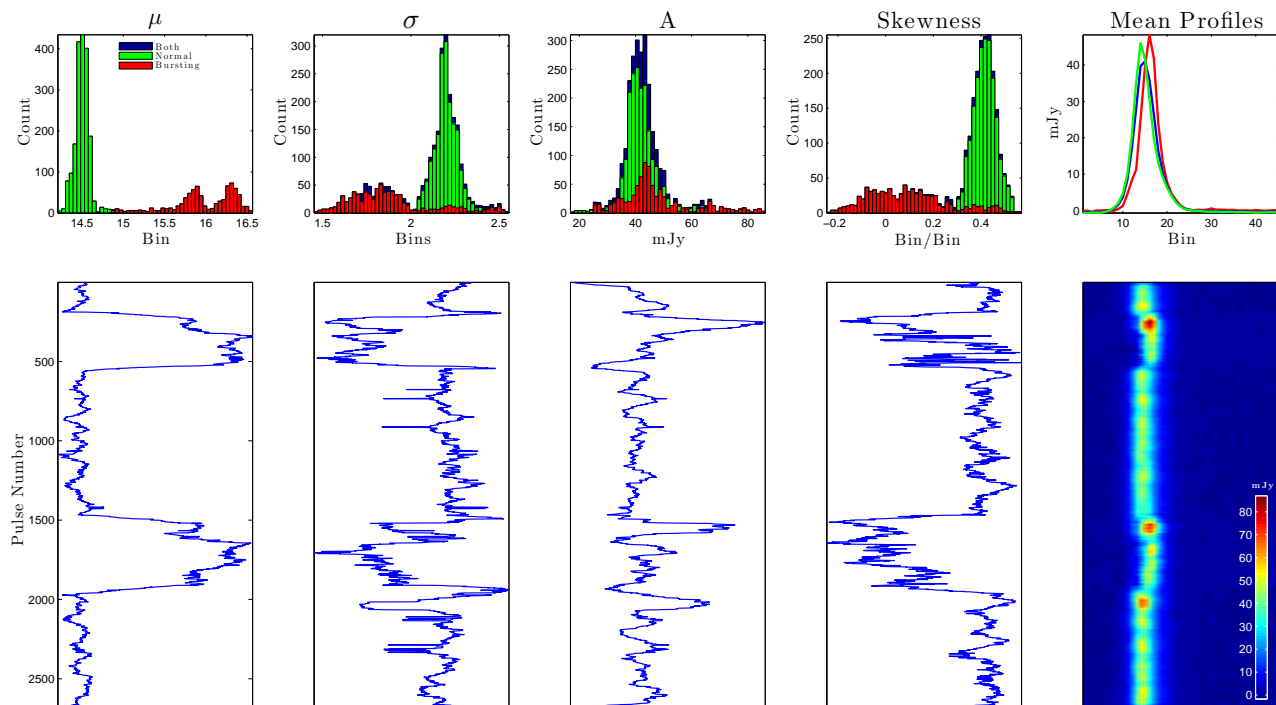


Figure 7. Gaussian parameters and skewness measurements of the smoothed data from the observation carried out on MJD 54898 at 327 MHz with the normal profile removed from the bursting modes.

In efforts to explain these varying trends, the 327 MHz observation is re-examined. The larger amplitude and similar width of the bursting pulse allows for a nested normal pulse to be simultaneously emitting. From the indexing of the previous analysis, we remove the mean normal-pulse for the bursting sequences in the raw data set. This new set is then convolved and Gaussian fitted to form Fig. 7. There we can see that the new trends reflect the ones observed at 1.4 GHz. Where the bursting pulses are narrower than the normal mode, and the amplitudes are of similar magnitude.

Mean profiles for each situation are presented in the far right hand corners of Fig. 5, 6, and 7. The bursting profiles for each are contained within the normal profile's starting and ending envelope. Therefore, it appears that the different emission mechanisms are confined to a single emission cone. This confinement is also supported by the skewness measurements, where the asymmetry of the profile is changing to accommodate for this restraint, as well as the phase changes.

3.3.2 Bursting rate

When the analysis from the previous section is performed on the other observations from Table 1, we find that bursting events are occurring rather frequently in this pulsar, with at least one mode shift per observation. All the observations support the same statistical trends in Fig. 5 and 6 for their respective bands. From the length of each burst and the total number of events over all the observations, we estimate a bursting event occurs approximately every seven minutes (1200 pulses) lasting for two to four minutes (300 - 600 pulses).

3.4 Pulse energy distributions

From the indexing in the previous sections, we are able to form sub-set pulse energy distributions for each mode. This was done by summing ten phase bins on either side of the maximum mean phase bin for each pulse in the raw data sets. A bin span was then converted to time and multiplied by the sum to produce an energy for each pulse. The energy distributions for each mode and the overall observation are then generated, see Fig. 8.

For the 327 MHz pulse energy distributions, a log-normal probability density function (PDF) is fitted for each mode with a maximum-likelihood estimation (mle). From these fits, shown in the left side of Fig. 8, both modes are well described by different log-normal distributions occupying different percentages (p) of the overall observation. Here we again see that the bursting pulses are more energetic, dominating the higher energies while the normal mode pulse are centralized at lower energies. When these two fits are summed and compared to the overall energy distribution, lowest left panel in Fig. 8, we can see that it matches very well to support that our indexing separates these two mode effectively.

When the same method was applied to the 1400 MHz observation, the log-normal fits did not provide a satisfactory fit to the data in the lower energy range. Because of this and the overall lower energy levels, we wanted to investigate whether the noise was effecting an underlying log-normal distribution. To incorporate this noise to a log-normal PDF, we needed to integrate the probability of other values (x') being read at another location (x) due to the Gaussian noise.

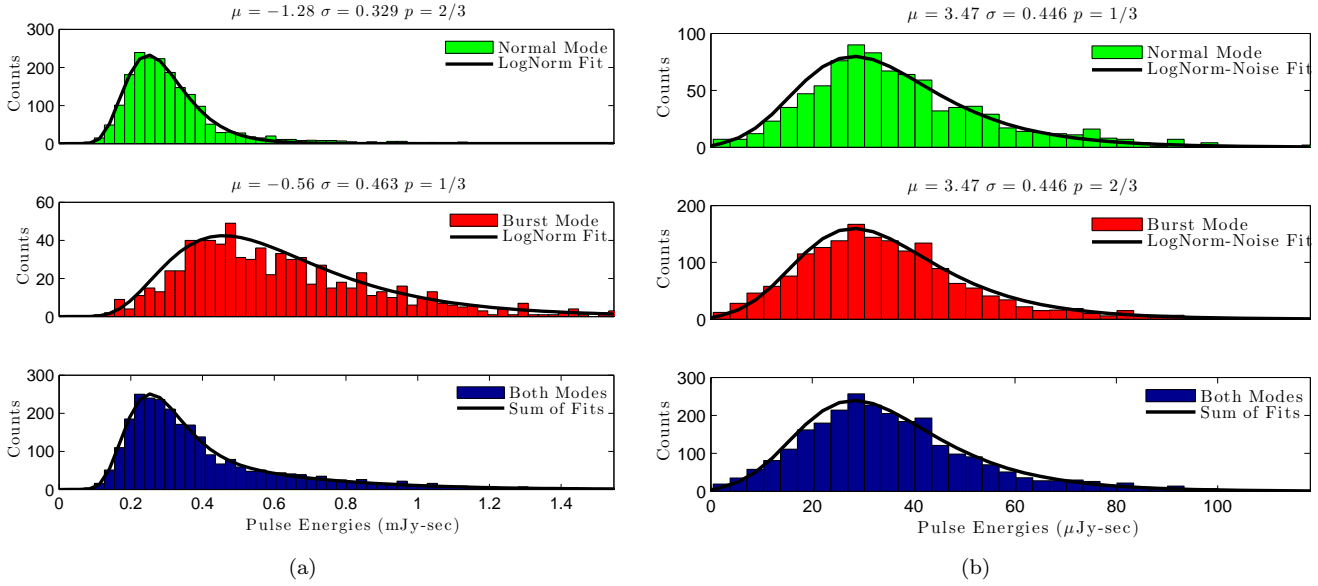


Figure 8. Pulse energy distributions for each mode and for entire observation. (a) The distributions for the 327 MHz observation on MJD 54898 with log-normal fits. (b) The distributions for the 1400 MHz observation on MJD 54898 with log-normal effected by noise fits.

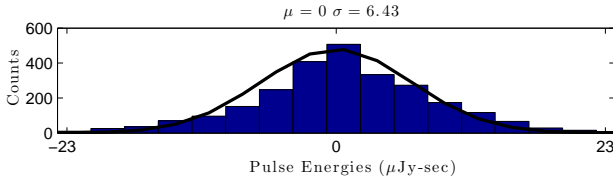


Figure 9. Off pulse energy distribution with a Gaussian fit.

Resulting

$$PDF(x) = \int_0^\infty \frac{1}{x' \sqrt{2\pi\sigma^2}} e^{-\frac{(\ln x' - \mu)^2}{2\sigma^2}} \frac{1}{\sqrt{2\pi\sigma_n^2}} e^{-\frac{(x-x')^2}{2\sigma_n^2}} dx', \quad (1)$$

where μ and σ are the shape parameters for the underlying log-normal and σ_n is the standard deviation of the Gaussian noise. Because of the symmetry of the Gaussian, this is the same as convolving the log-normal with a normal distribution.

To find a value for σ_n , we summed and converted 21 bins in the off-pulse region, then fitted a Gaussian to this energy distribution, shown in Fig. 9. We repeatedly found that the energies in the off-pulse regions were well described with $\sigma_n = 6.43 \mu\text{Jy-sec}$.

Unfortunately, the PDF in Eq. 1 has no analytical solution. Therefore, we approximate this with an finite intervals summation and use these values as our new PDF for the mle fitting. These fits matched the distribution remarkably well, now describing the whole distribution with little change in the log-normal shape parameters, shown in the right side of Fig. 8.

There we can see that both modes can be described with at single energy distribution. This supports what was seen in the previous sections, that there was little change in the amplitudes of the pulses between the two modes. What is peculiar, is that the pulse width changes between the modes

are not significant enough to be reflected in the energies. This maybe because of the noise contribution.

3.5 Sub-pulse drifting analysis

We now take the opportunity to revisit the issue of the presence of any sub-pulse drifts in the two emission states of B0611+22. If sub-pulse drifts are occurring with regular frequency, there should be a dominant peak in the Fourier transform of each phase bin of the raw data (Backer 1970a,b). While this analysis has been performed on this pulsar before in Weltevrede et al. (2006, 2007) with no features found, the two modes have not been looked at independently. Therefore, we investigate each mode separately to see if any differences can be seen in the frequency domain. Because we are only interested in the fluctuations of the profile, the mean value of each phase bin is subtracted before calculating a fluctuation spectra.

When investigating amplitudes of the first bursting event at 327 MHz, shown in the left hand side of Fig. 10, it soon becomes evident that the lower frequencies are playing a dominant roll. To examine why this is, we first produce a linear fit of the mean intensities of each pulse number. This fit is then Fourier transformed and compared to the the mean amplitude of each frequency in the data, shown in the upper right hand side of Fig. 10. We can then see that in the low frequency range these two spectra are comparable. This suggests that these low frequencies are a consequence of the large scale structure of the bursting envelope.

To see if any radio interference is contributing, the fluctuation spectra of an off-pulse region of the same area is taken for comparison. The mean value of this region is plotted in the upper right hand side of Fig. 10, where a single signal is seen at high frequency. This radio interference does not seem to be a major contributor. Regardless, this and the linear trend spectra are subtracted from the mean

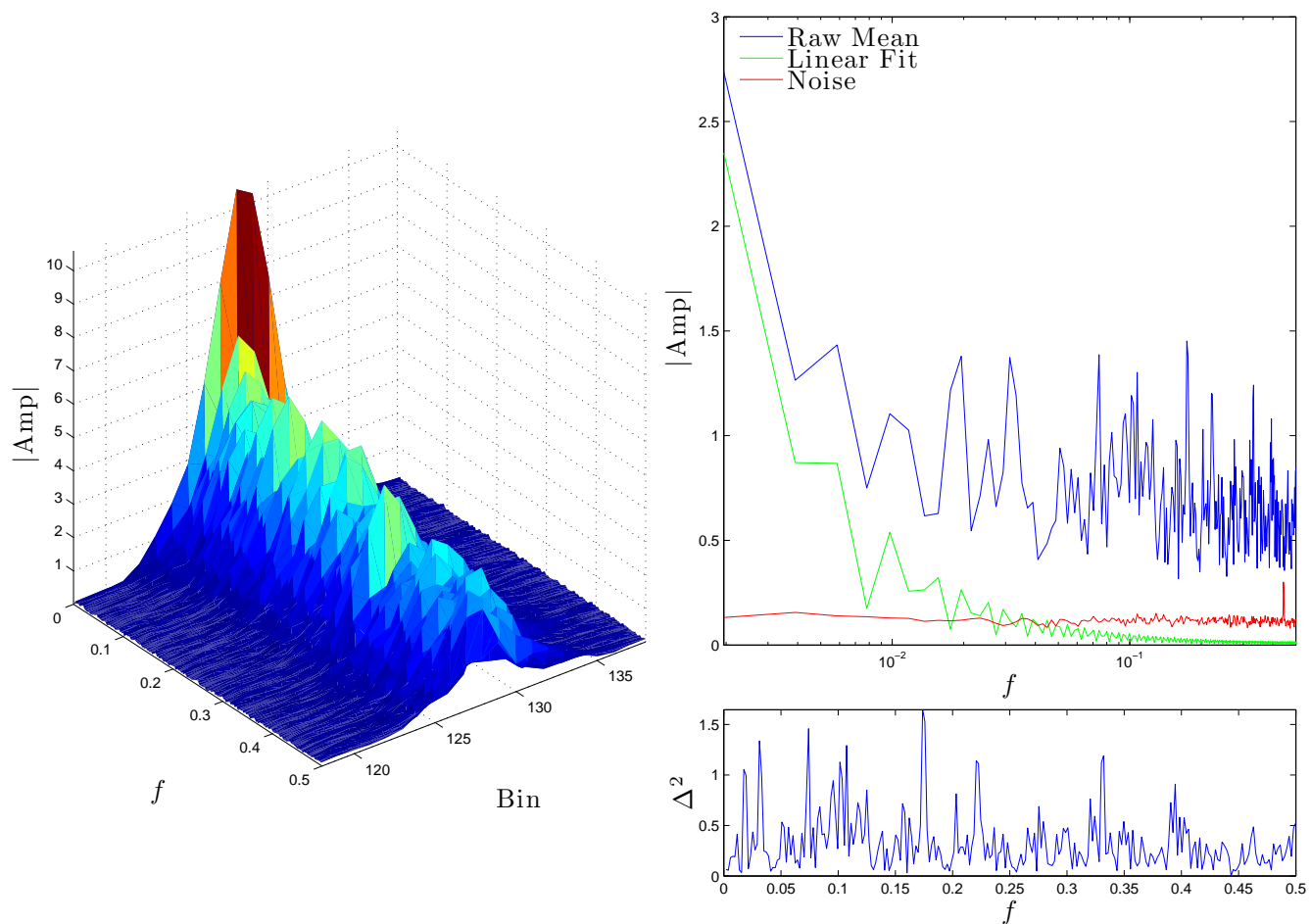


Figure 10. (Left) The fluctuation spectra of the first bursting event for 327 MHz in Fig. 1, covering 21 bins centred on the mean peak and from pulse-numbers 220 to 530. (Upper Right) The mean amplitude of each frequency of the *Left* figure. Along with the Fourier transform of a linear fit of the mean flux from the same section in Fig. 1, and the mean amplitude of frequencies from an off pulse area of the same size. (Lower Right) The squared of the difference of raw mean amplitude from the amplitudes of the linear fit and the mean off source. Here all frequencies (f) are in cycles-per-period (C/P).

data spectra. This difference in amplitudes is then squared to approximate how the other components are contributing to the power, seen in the lower right of Fig. 10. There we can see that there are no substantial single frequency peaks, suggesting that sub-pulse drifting is not prevalent in this mode. When the same procedure is conducted on the normal mode (Fig. 11), there is clearly no low frequency dominance as what was seen in the bursting mode. This is consistent with the structural explanation since the normal mode should have no large-scale pattern. Again we see no prominent peaks in the amplitude difference.

These results are consistent with what was reported in Weltevrede et al. (2006, 2007). This analysis does suggest however, that if a ‘red noise’ component in the fluctuation spectra it may be a sign of intrinsic structures in the intensity and should not always be disregarded as interstellar scintillation or receiver fluctuations (Lorimer & Kramer 2005).

4 PREDICTIONS FOR OBSERVATIONS AT X-RAY WAVELENGTHS

Another very interesting possibility is that PSR B0611+22, and others like it, may be detectable as X-ray state switching pulsars, as was recently demonstrated for the classical mode-changing pulsar B0943+10 where non-thermal unpulsed X-rays are observed during the bright radio emitting phases, while an additional pulse thermal component is present during the radio quiet phase (Hermesen et al. 2013). A comparison between Fig. 1 of this paper and Fig. 1 of Hermesen et al. shows that the radio properties of PSRs B0611+22 and B0943+10 are reversed: for B0611+22 we see a burst and decay behavior, while for B0943+10 the bright mode gradually increases in strength before declining rapidly to the radio-quiet state. Correlated radio and X-ray observations would allow us to see the energy ranges over which this pulsar is switching between emission states. In this section, we make some testable predictions for future radio and X-ray observations of PSR B0611+22.

If PSR B0611+22 behaves in a similar way to PSR B0943+10, then we expect a higher level of X-ray emission, accompanied by spectral changes, during its non-

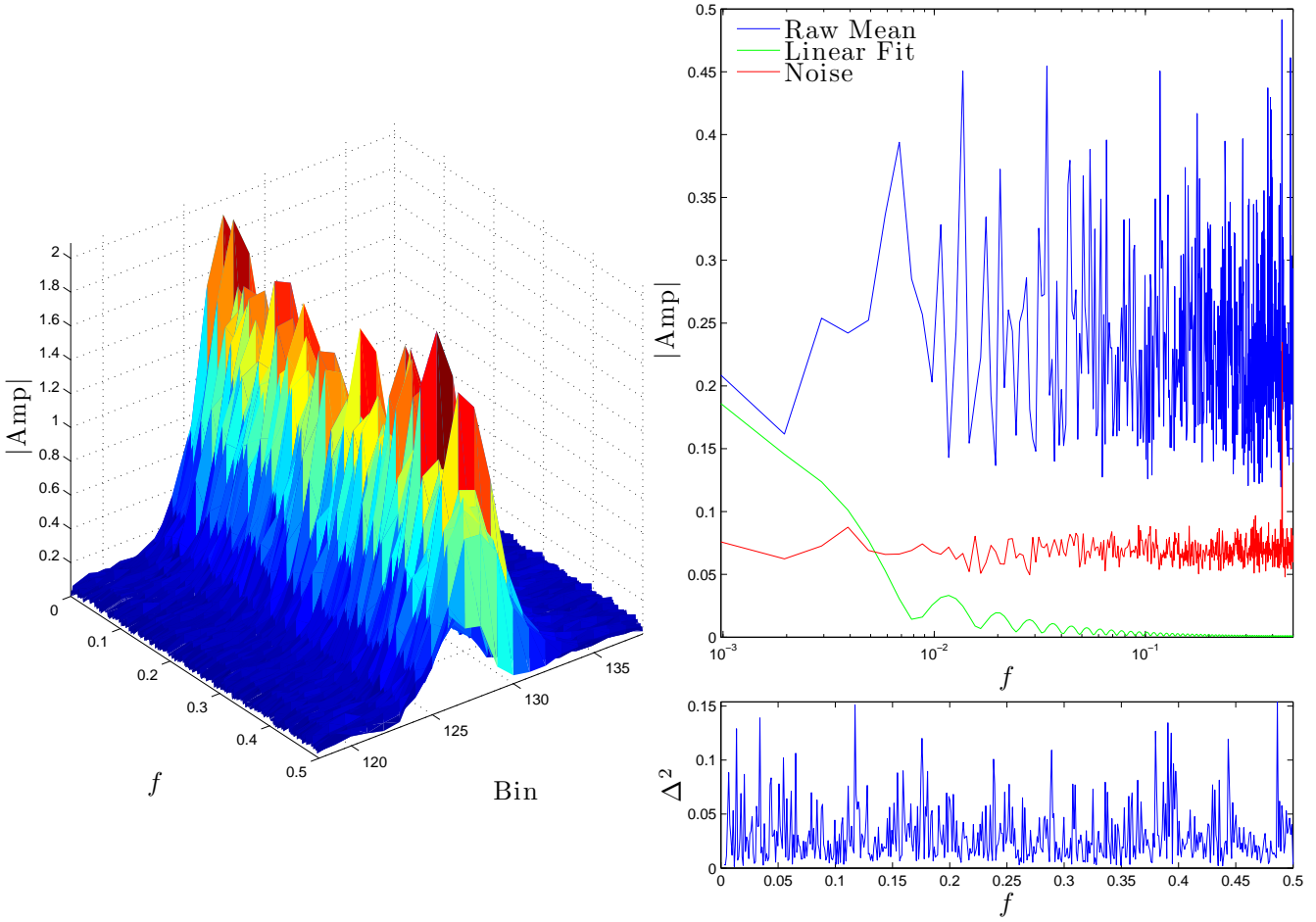


Figure 11. (Left) The fluctuation spectra of the longest normal mode for 327 MHz in Fig. 1, covering 21 bins centred on the mean peak and from pulse-numbers 550 to 1450. (Upper Right) The mean amplitude of each frequency of the *Left* figure. Along with the Fourier transform of a linear fit of the mean flux from the same section in Fig. 1, and the mean amplitude of frequencies from an off pulse area of the same size. (Lower Right) The squared of the difference of raw mean amplitude from the amplitudes of the linear fit and the mean off source. Here all frequencies (f) are in cycles-per-period (C/P).

bursting radio phases. Although PSR B0611+22 is more distant than PSR B0943+10, its higher spin-down energy loss rate³ (6.2×10^{34} ergs s⁻¹ versus 1.0×10^{32} ergs s⁻¹) provides excellent prospects for the detection of both thermal and non-thermal X-ray emission. To estimate the non-thermal X-ray flux expected from PSR B0611+22, F_X^{nt} , we assume an X-ray efficiency of 1%, as inferred for PSR B0943+10 from Hermsen et al. (2013), and a dispersion measure distance of 4.7 kpc and find that $F_X^{\text{nt}} = 3.8 \times 10^{-13}$ ergs s⁻¹ cm⁻². To estimate thermal X-ray flux, F_X^{th} , we use the recent compilation of kT versus characteristic age presented in Fig. 1 of Keane et al. (2013) to infer $kT = 120$ eV for PSRs B0611+22. Assuming blackbody radiation from a region around the polar caps of an $R = 10$ km radius neutron star we can estimate the thermal X-ray flux, F_X^{th} . For the purposes of this calculation, we have adopted an emitting region with a radius of 2.7 polar cap radii.⁴ At the

nominal dispersion measure distance of 4.7 kpc, we find $F_X^{\text{th}} = 3 \times 10^{-15}$ ergs s cm⁻².

These anticipated X-ray fluxes translate into reasonably high count rates with existing X-ray instruments. For example, using the *pimms* simulation package, the expected count rates for the *XMM* PN instrument are approximately 0.05 s⁻¹ for the non-thermal emission (assuming a power-law spectrum with a photon index of 2) and 0.001 s⁻¹ for the blackbody emission. These count rates are very encouraging and translate into detections of up to a few hundred photons per source. The different spectral properties of the thermal and non-thermal emission, and the simultaneous radio monitoring, will allow the discrimination between thermal and non-thermal emission for each emission mode. For example, assuming a 30% bursting duty cycle for PSR B0611+22 and the same X-ray properties as B0943+10, our count-rate estimates translate to detections of ~ 20 thermal photons plus ~ 1000 non-thermal photons during the non-bursting

³ Following standard practice (see e.g. Lorimer & Kramer 2004), we compute the spin-down energy loss rate $\dot{E} = 3.95 \times 10^{31} \text{ ergs s}^{-1} \dot{P}_{-15} / P^3$ for the spin period P in s and $\dot{P}_{-15} = 10^{15} \dot{P}$.

⁴ This choice was motivated by the fact that the thermal emission

observed in B0943+10 is consistent with a circular region of radius 370 m. The classical (see, e.g. Lorimer & Kramer 2005) polar cap radius for this pulsar, $R\sqrt{2\pi R/(Pc)}$, is 140 m.

state, and ~ 500 non-thermal photons during the bursts. The number of non-thermal photons detected may be lower if the above 1% efficiency assumption is an overestimate. In either case, however, the excellent statistics provided by the thermal photons means that it should be possible to readily distinguish between changes in the X-ray luminosity and/or spectra in the normal and bursting radio states.

5 CONCLUSION

In summary, using a sensitive boxcar convolution method to preserve the phase resolution, we have found exceptional pulse patterns in the radio emissions from PSR B0611+22 in archival data taken with the Arecibo radio telescope.

With this analysis, prolonged enhanced emissions were discovered at 327 MHz. When investigating the overall structure of this emission, it was shown that these are bursting events that abruptly appear and then systematically decay. These events appear to be superimposed upon a constant emission mode offset in pulse phase. This was unexpected and is a completely undocumented relationship for this pulsar.

To gain further insight into these events, we searched for them at 1.4 GHz using the same method, finding a different picture compared to 327 MHz. At 1.4 GHz, the bursting events were no longer bright episodes, and the steady emission mode was no longer present. At this frequency PSR B0611+22 appears to be a mode switching pulsar, where one mode is the decaying burst and the other mode is constant when on. This mode switching is surprising in this pulsar, only being suggested briefly in the past (Nowakowski 1992; Nowakowski & Rivera 2000). PSR B0611+22's characteristic age is also surprising, because the majority of mode-switching pulsars are a couple of orders of magnitude older (Wang et al. 2007). This age discrepancy may suggest that bursting pulsars are a new classification of pulsars that are independent of nulling and moding.

To investigate these relationships, we fitted Gaussians and measured the skewness of each convolved pulse. These measurements allowed us to confirm that there was a phase change between the two modes. This was used to isolate each of the mode statistics in each frequency range. We then showed, that the parameter differences were reflected in each mode's mean profile. These mean profiles, along with the skewness measurements, support that the modes are confined to the same phase region and therefore the same emission cone.

This analysis also shows that, apart from the amplitude difference from 327 to 1400 MHz, there was also a change in the distribution of the pulse-width parameters. To see what could be causing this distribution change, we revisited the 327 MHz data and subtracted the constant underlying emission from the burst. When this was done, the normal mean profile from the 327 MHz bursting event distributions became consistent with the 1.4 GHz distributions.

An investigation of the pulse energy distributions also revealed differences between the two modes. While both modes can be described by log-normal probability density functions, at 327 MHz the modes are independent, but at 1400 MHz both mode energies are in a single function.

The two modes were also searched for drifting sub-

pulses independently, where no significant signals were present in any of the fluctuation spectra, supporting Weltevrede et al. (2006, 2007) that sub-pulses are not prevalent in this pulsar. We have also shown that if B0611+22 acts similarly to other known pulsars, it could exhibit changes in its X-ray luminosity between the two separate modes. PSR B0611+22 is particularly attractive as a potential X-ray source due to its relative youth. Correlated radio and X-ray observations are being planned for 2014.

It is interesting to note that PSR B0611+22 does exhibit period derivative variations in a manner analogous to those published by Lyne et al. (2010; A.G. Lyne, private communication based on Lovell radio telescope observations). It is currently an open question as to whether these changes are related to the bursting events we see here. Perhaps the pulsar bursts only in one of the spin-down rate changes? Our data, sampled on only a few days, are insufficient to answer this question. Further detailed studies are required.

Before this analysis, the curious emission properties of B0611+22 were not well known (Nowakowski 1992). Because this is the first pulsar that we have tried with this analysis, this may be a more common occurrence than we realise. In particular this work required the unique sensitivity of the Arecibo telescope to reveal this behaviour. Further studies of this kind are clearly necessary.

On a more global scale, studies such as this can help draw relationships between different types of modal and emission variations. Here it is easy to imagine a threshold situation that can relate nulling and bursting events. Consider, for example, similar pulsars to B0611+22 that are either not as bright or are farther away such that the normal mode is undetected. In this case the normal mode would be interpreted as being in a null state. A similar argument was made for PSR B0656+14 in the context of a possible connection with rotating radio transients Weltevrede et al. (2006). Further examples of this phenomenon will allow us to build up a more complete picture of the complex emission phenomenology of radio pulsars.

ACKNOWLEDGMENTS

The Arecibo Observatory is operated by SRI International under a cooperative agreement with the National Science Foundation (AST-1100968), and in alliance with the Ana G. Méndez-Universidad Metropolitana, and the Universities Space Research Association. This work was supported by grants from West Virginia EPSCoR, the Research Corporation for Scientific Advancement and the National Science Foundation PIRE award (OISE 0968296). We made use of the facilities of the ATNF Pulsar Catalogue. Computer resources used during the later stages of this project were supported from a WV EPSCoR Challenge Grant. DRL acknowledges support from Oxford Astrophysics while on sabbatical leave. We thank Aris Karastergiou, Maura McLaughlin, Andrew Lyne, Patrick Weltevrede, Ben Stappers and the referee, Geoff Wright, for useful comments.

REFERENCES

- Backer D. C., 1970a, *Nature*, 228, 752
 Backer D. C., 1970b, *Nature*, 227, 692
 Backer D. C., 1970c, *Nature*, 228, 1297
 Backer D. C., 1970d, *Nature*, 228, 42
 Backer D. C., Boriakoff V., Manchester R. N., 1973, *Nature Physical Science*, 243, 77
 Camilo F., Ransom S. M., Chatterjee S., Johnston S., Demorest P., 2012, *ApJ*, 746, 63
 Chandler A. M., 2003, Ph.D. thesis, California Institute of Technology
 Davies J. G., Lyne A. G., Seiradakis J. H., 1972, *Nature*, 240, 229
 Dowd A., Sisk W., Hagen J., 2000, in *Astronomical Society of the Pacific Conference Series*, Vol. 202, Kramer M., Wex N., Wielebinski R., ed, IAU Colloq. 177: Pulsar Astronomy - 2000 and Beyond, p. 275
 Drake F. D., Craft H. D., 1968, *Nature*, 220, 231
 Ferguson D. C., Boriakoff V., 1980, *ApJ*, 239, 310
 Helfand D. J., Taylor J. H., Backus P. R., Cordes J. M., 1980, *ApJ*, 237, 206
 Hermsen W. et al., 2013, *Science*, 339, 436
 Huguenin G. R., Taylor J. H., Troland T. H., 1970, *ApJ*, 162, 727
 Kramer M., Lyne A. G., O'Brien J. T., Jordan C. A., Lorimer D. R., 2006, *Science*, 312, 549
 Lewandowski W., Wolszczan A., Feiler G., Konacki M., Sołtysiński T., 2004, *ApJ*, 600, 905
 Lorimer D. R., Camilo F., McLaughlin M. A., 2013, *MNRAS*, submitted
 Lorimer D. R., Kramer M., 2005, *Handbook of pulsar astronomy*, Vol. 4. Cambridge University Press, Cambridge, UK
 Lorimer D. R., Lyne A. G., McLaughlin M. A., Kramer M., Pavlov G. G., Chang C., 2012, *ApJ*, 758, 141
 Lyne A., Hobbs G., Kramer M., Stairs I., Stappers B., 2010, *Science*, 329, 408
 Manchester R. N., Hobbs G. B., Teoh A., Hobbs M., 2005, *AJ*, 129, 1993
 McLaughlin M. A. et al., 2006, *Nature*, 439, 817
 Nowakowski L. A., 1992, in *Hankins T. H., Rankin J. M., Gil J. A., ed, IAU Colloq. 128: Magnetospheric Structure and Emission Mechanics of Radio Pulsars*, p. 280
 Nowakowski L. A., Rivera N. S., 2000, in *Bulletin of the American Astronomical Society*, Vol. 33, American Astronomical Society Meeting Abstracts
 Rankin J. M., Rodriguez C., Wright G. A. E., 2006, *MNRAS*, 370, 673
 Rankin J. M., Stinebring D. R., Weisberg J. M., 1989, *ApJ*, 346, 869
 Seymour A. D., Lorimer D. R., 2013, *MNRAS*, 428, 983
 Unwin S. C., Readhead A. C. S., Wilkinson P. N., Ewing W. S., 1978, *MNRAS*, 182, 711
 Wang N., Manchester R. N., Johnston S., 2007, *MNRAS*, 377, 1383
 Weisberg J. M. et al., 1999, *ApJS*, 121, 171
 Weltevrede P., Edwards R. T., Stappers B. W., 2006, *A&A*, 445, 243
 Weltevrede P., Stappers B. W., Edwards R. T., 2007, *A&A*, 469, 607
 Weltevrede P., Stappers B. W., Rankin J. M., Wright

G. A. E., 2006, *ApJ*, 645, L149

APPENDIX A: SKEWNESS EQUATIONS

$$\mathcal{S} \equiv \mathbb{E} \left[\left(\frac{x - \mathbb{E}[x]}{\text{std}[x]} \right)^3 \right]. \quad (\text{A1})$$

Here x is a bin value, $\mathbb{E}[x]$ is the mean value of x and $\text{std}[x]$ is its standard deviation.

In this paper we treat each local mean pulse as a distribution function and use the flux densities (y_x) for a weighted average. We define our weighting (w_x) as

$$w_x \equiv \frac{y_x}{\sum y_x}. \quad (\text{A2})$$

This then produces a weighted-mean value of

$$\mathbb{E}[f_x] = \sum f_x w_x. \quad (\text{A3})$$

Here f_x is a function of x . Using this definition we write the standard deviation as

$$\text{std}[f_x] = \sqrt{\mathbb{E}[f_x^2] - \mathbb{E}[f_x]^2}. \quad (\text{A4})$$

The skewness is then calculated with an expansion of its definition, i.e.

$$\mathcal{S} = \frac{\mathbb{E}[x^3] - 3\mathbb{E}[x]\text{std}[x]^2 - \mathbb{E}[x]^3}{\text{std}[x]^3}. \quad (\text{A5})$$